Preserving Vorticity Improves the Accuracy of Multiscale Solvers

H. Ali Marefat[a], Muhammad A. Ashjari Aghdam[b], Knut-Andreas Lie[c]

[a]*Mechanical, Electrical and Computer Engineering Department, Science and Research Branch, Islamic Azad University, Tehran, Iran*
[b]*Mechanical Engineering Department, Jolfa International Branch, Islamic Azad University, Aras Free Zone, East Azerbaijan, Iran*
[c]*SINTEF Digital, Mathematics and Cybernetics, Oslo, Norway*

Abstract

Within reservoir management, there is a growing demand for highly accurate and fast reservoir simulators. So-called multiscale methods are designed to preserve fine-scale information accurately in an accelerated coarse-scale computation of fluid flow. In many cases, this requires that coarse partitions are meticulously adapted to prominent geological features that determine flow paths. Partitions that seek to preserve the vorticity from a representative fine-scale flow simulation can be particularly effective to this end. We describe how to incorporate such partitions in the state-of-the-art multiscale restriction-smoothed basis (MsRSB) method, and present a series of two-phase test cases to validate and demonstrate the effectiveness of the resulting method. Our results show that using a nonuniform vorticity-based partition improves the accuracy of the MsRSB solver compared with uniform partitions and nonuniform partitions with a similar number of coarse blocks that adapt to permeability or velocity.

Keywords: Vorticity preservation theory, adaptive grid, unstructured grid, multiscale simulation, restriction-smoothed basis.

1. Introduction

So-called multiscale methods have been developed to systematically and correctly account for how fine-scale variations in rock parameters affect flow on a coarser scale. The literature contains various classes of multiscale methods such as multiscale finite-element methods [1], numerical subgrid upscaling [2, 3], mixed multiscale finite-element methods [4, 5], multiscale finite-volume methods [6], mortar mixed finite-element methods [7], and multiscale mimetic methods [8] to name a few. Lie et al. [9] give a more comprehensive overview that focuses on methods applicable to practical reservoir simulation.

Most of these methods utilize two grids: a fine grid describing the rock parameters of the reservoir and a coarse partition imposing global flow equations. The main idea is to construct a numerical mapping between the degrees of freedom on the coarse and the fine grid by solving fine-scale flow problems localized to a small area surrounding each block in the coarse grid. The local flow solutions are called *multiscale basis functions* and represent, in a finite-volume formulation, how the effect of a unit pressure prescribed at one block center would distribute itself locally, given zero pressure at the centers of the neighboring blocks. Each basis function gives a mapping between the degree of freedom associated with the coarse block and the fine-scale degrees of freedom inside the support of the basis function. By collecting the local basis functions into a global mapping, we get a systematic means to introduce fine-grid information into a set of reduced-order, coarse-scale flow equations. Originally, multiscale methods were designed as a robust alternative to *upscaling* [10, 11, 12]. They resolve global flow patterns on the coarse grid with at least the same accuracy as state-of-the-art local-global upscaling methods [13, 14] and with much better accuracy than traditional averaging and local flow-based methods, e.g., as evidenced in [15]. However, most multiscale methods also offer some means to *reconstruct* a conservative flow field on the underlying fine grid, either by exploiting the subresolution inherent in the basis functions or by solving another local flow problem. Herein, we consider one specific multiscale method, the MsRSB method [16, 17], which represents state-of-the-art as recently implemented in a commercial simulator with for 3-phase black-oil equations [18, 9]. The MsRSB method is very versatile and can, for instance, be formulated for a wide class of coarse partitions in which the coarse blocks are made up of almost arbitrarily shaped, connected aggregates of polyhedral cells.

The number of floating-point operations for a full multiscale solve (computing basis functions, assembling and inverting the reduced-order system, reconstructing fine-scale approximation) can be shown to be approximately the same as for an efficient linear solver applied directly to the original fine-scale problem [15]. When used as a preconditioner in an iterative framework, multiscale methods are approximately as efficient as state-of-the-art algebraic multigrid solvers and scale very well on parallel architectures; see [19, 20, 21] for more details. The main advantage of using a multiscale method can be observed for multiphase and transient flow problems, for which it is necessary to update the pressure repeatedly. In many flow scenarios, the temporal dependence in pressures and fluxes is moderate compared to the spatial variability, and temporal changes are often localized. Multiscale methods exploit this fact and will reduce the overall computational cost significantly compared with a fine-scale simulation if we reuse previously computed basis functions from one time step (or iteration) to the next. Likewise, improved computational efficiency can be observed if the multiscale method is used as an approximate solver that reduces the fine-scale residual below a prescribed, relaxed tolerance and at the same time guarantees a mass-conservative approximation [16]. Typically, multiscale methods reduce computational costs by one order of magnitude for flow problems with highly heterogeneous rock properties.

Solving flow equations on a coarser grid introduces numerical errors [22, 23]: upscaling errors arise because homogenization of the medium inside each coarse block smooths the rock parameters, whereas using a coarser grid increases the spatial discretization error. Previous research has shown that upscaling errors are reduced if one applies coarse grids that adapt to the (flow) characteristics of the underlying geological model [24]. The same holds true for multiscale methods in general, and for MsRSB in particular [25]. As a simple heuristic, one can imagine that it would be possible to minimize discretization errors for a given cell count by employing higher grid resolution in regions with high flow rates or where the flow has large spatial variations and lower grid resolution in regions with slow flow or small changes. Coarsening differently in the near-well, high-flow, and far-field regions could be one such approach [26]. Likewise, upscaling errors could be minimized by grouping cells with similar petrophysical parameters and distinguishing cells with largely different parameters.

Coarsening techniques based on agglomeration apply cell-based indicator functions to group similar cells into aggregates and separate cells that are distinctively different. The literature discusses various types of indicators: Permeability techniques group cells with similar values of permeability [23], techniques based on velocities or time-of-flight generate coarse grids that adapt to flow patters, typically with higher grid resolution in regions with high flow [27, 28, 29, 30]. Vorticity techniques try to preserve regions with high-vorticity values and group cells in regions with low-vorticity values [31, 32, 33], and have proved to be very effective in generating optimum coarse-scale grids [34, 35].

In this paper, we propose to combine the MsRSB method with a vorticity-based coarsening technique. That is, we propose to solve a single-phase flow problem to generate a vorticity map and then use this to define the coarse partition required by the MsRSB method. We investigate and demonstrate the efficacy of the resulting method, which we refer to as VMsRSB, through a series of two-phase simulation: a simple lens model, layers sampled from Model 2 of the 10th SPE Comparative Solution Project (SPE10) [36], as well as two 3D models representing the Norne oil and gas field and parts of the Johansen formation from the Norwegian Continental Shelf.

2. Model Equations

Multi-fidelity simulators normally need to cover a wide range of flow and recovery processes, and the particular multiscale method discussed herein has been successfully applied to study industry-grade black-oil models [17, 18, 9], polymer flooding with non-Newton rheology [37], embedded fracture models [38], and compositional simulation [39]. Similar multiscale methods, but with a different method of computing basis functions, have been applied to other types of processes like discrete fracture models [40, 41], geothermal flow [42], geomechanics [43], and coupled flow and geomechanics [44], to name a few. However, to demonstrate how using vorticity preservation improves the accuracy of the basic multiscale method, it is sufficient to only consider incompressible, immiscible, two-phase flow. In the absence of gravity and capillary forces, this system is described by an elliptic Poisson-type equation for fluid pressure p and a hyperbolic equation for fluid saturation S, coupled through the total Darcy velocity $\vec{v}_t$:

$$\nabla \cdot \vec{v}_t = q_t, \qquad \vec{v} = -\mathbf{K}\lambda_t(S)\nabla p, \tag{1}$$

$$\phi \frac{\partial}{\partial t} S + \nabla \cdot (f \vec{v}_t) = q. \tag{2}$$

Here, $\mathbf{K}$ and ϕ denote permeability and porosity, $\lambda_t(S)$ is the total mobility of the two-phase composition, and f and q denote the fractional flow and the flow rate of the volumetric source for the wetting phase. These equations are defined over a closed and connected domain, represented by a grid consisting of volumetric cells $\Omega_i, i = 1, \ldots, n$. To discretize Eqs. (1) and (2), we introduce a standard finite-volume method for the cell-averaged pressure p_i and saturation S_i in cell Ω_i, formulated with two-point flux approximation and upstream weighting of saturation-dependent coefficients. That is, the discretized pressure equation (1) with fixed saturation reads,

$$\sum_{j \in \mathcal{N}(i)} v_{ij} = q_i, \qquad v_{ij} = \lambda_t(S)_{ij} T_{ij} (p_i - p_j), \tag{3}$$

where $\mathcal{N}(i)$ holds the indices of the neighbors of cell i, and T_{ij} denotes the transmissibility between cells i and j, defined as

$$T_{ij} = 1/\big(T_{i,j}^{-1} + T_{j,i}^{-1}\big), \qquad T_{i,j} = A_{ij} \frac{(\mathbf{K}_i \vec{c_{i,j}}) \cdot \vec{n}_{i,j}}{|\vec{c}_{i,j}|^2}. \tag{4}$$

Here, A_{ij} is the area of the interface Γ_{ij} between cells i and j, $\vec{n}_{i,j}$ is the normal vector pointing from cell i to cell j, and $\vec{c}_{i,j}$ is the vector between the centroids of Ω_i and Γ_{ij}. For the mobility term, we use upstream weighting, i.e.,

$$\lambda_t(S)_{ij} = \begin{cases} \lambda_t(S_i) & \text{if } T_{ij}(p_i - p_j) > 0, \\ \lambda_t(S_j) & \text{otherwise.} \end{cases} \tag{5}$$

Likewise, the saturation equation is discretized as follows:

$$\frac{S_i^{n+1} - S_i^n}{\Delta t} + \frac{1}{\phi_i |\Omega_i|} \sum_{j \in \mathcal{N}(i)} v_{ij} f(S)_{ij}^{n+1} = \max(q_i, 0) + \min(q_i, 0) f(S_i^{n+1}), \quad (6)$$

where n denotes discrete time levels, Δt is the time step, and

$$f(S)_{ij} = \begin{cases} f(S_i) & \text{if } v_{ij} > 0, \\ f(S_j) & \text{otherwise.} \end{cases} \quad (7)$$

The combined system is solved sequentially, one time step at the time, by first solving (3) with S fixed, and then solving (6) with v_{ij} fixed.

3. The Multiscale Method

In this section, we first briefly outline the multiscale method for the discrete pressure equation (3), which we in the case of single-phase flow can write as,

$$Ap = q. \quad (8)$$

The solution of this system will henceforth be considered as our true solution, to which we compare all other solutions. After we have outlined the basics of the multiscale method, we explain the vorticity preservation theory used to partition the fine grid into coarse blocks.

3.1. Multiscale Restriction-Smoothed Basis (MsRSB)

To define the multiscale method, we need a fine-scale grid $\{\Omega_i\}_{(i=1)}^n$ and a coarse partition, represented as a vector P of length n. The partition is defined such that grid cell Ω_i belongs to coarse block $\overline{\Omega}_k$ if and only if $P(i) = k$, and each grid cell belongs to only one block in the coarse partition. As a mental picture, you can think of a 10×10 Cartesian grid that is partitioned into a 5×5 coarse grid so that each coarse block consists of 2×2 fine cells.

Multiscale finite-volume methods use a prolongation operator (collection of local basis functions) to map quantities defined on the coarse grid to quantities on the fine grid, i.e., $\mathcal{P} : \{\overline{\Omega}_j\} \rightarrow \{\Omega_i\}$. An analogous restriction operator maps quantities from the fine-scale to the coarse-scale, i.e., $\mathcal{R} : \{\Omega_i\} \to \{\overline{\Omega}_j\}$. For a grid with n cells partitioned into m coarse blocks, these operators can be represented as sparse $n \times m$ and $m \times n$ matrices, respectively. The simplest way to define $\mathcal{P}$ would be to let each column represent the characteristic function of the corresponding coarse block, i.e., set $\mathcal{P}_{ik} = 1$ if $P(i) = k$, and $\mathcal{P}_{ik} = 0$ otherwise. (Likewise, we set $\mathcal{R}_{ki}$ equal one if $P(i) = k$, and zero otherwise.)

The MsRSB method seeks to define an algebraically smooth prolongation operator $\mathcal{P}$. That is, starting with each column of $\mathcal{P}$ defined as the characteristic function of the corresponding coarse-scale block, we apply an inexpensive localized iterative scheme, e.g., a Jacobi iteration based directly on the fine-scale discretization matrix A, to gradually smooth $\mathcal{P}$ so that it becomes increasingly consistent with the local properties of the elliptic differential operator $\nabla \cdot \mathbf{K}\nabla$. Each new iteration grows the support of the basis function (column of $\mathcal{P}$) outward from its associated block. This continues until the support reaches the perimeter of a prescribed support region, at which point a lumping procedure is applied to ensure that the basis functions stay localized and together represent a partition of unity, i.e., so that each row of $\mathcal{P}$ sums to one; see [16] for more details. After a certain number of iterations, the basis functions are algebraically smooth and can be used to map degrees of freedom between the fine and coarse grids in a consistent manner.

Assuming that we know a coarse-scale pressure solution p_c, we can define an approximate fine-scale pressure by use of the prolongation operator:

$$p_f = \mathcal{P} p_c. \tag{9}$$

Inserting the fine-scale approximation in (9) into (8), and applying the restriction operator $\mathcal{R}$, which essentially sums the local equations for all cells inside a coarse block, we obtain the reduced-order multiscale system defined over the coarse grid:

$$\mathcal{R}(A(\mathcal{P}p_c)) = (\mathcal{R}A\mathcal{P})p_c = A_c p_c = \mathcal{R}q = q_c. \tag{10}$$

Figure 1 summarizes the multiscale framework and compares it to a traditional fine-scale solver. The figure also illustrates precisely in which step the adapted,

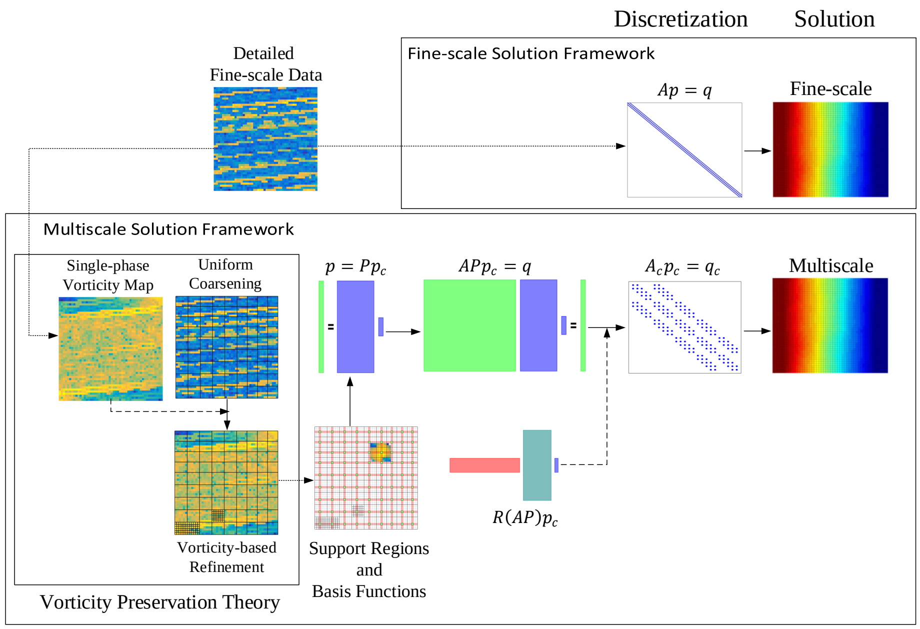

Figure 1: A schematic flowchart of the conventional fine-scale (the upper box) and VMsRSB (the lower box) simulation frameworks.

vorticity-based. coarse partition to be discussed in the next subsection is applied in the multiscale method.

With obvious modifications, we can easily extend the same idea to two-phase flow if we use a sequential solution procedure that solves pressure equations on the form $A(S)p = q$ for fixed S. For simplicity, we herein only compute the prolongation operator $\mathcal{P}$ once using a total mobility defined from the initial saturation distribution. This is arguably a good approximation as long as $\lambda_t(S)$ changes smoothly in time. To account better for more abrupt changes in total mobility, one can, if necessary, reiterate a few extra times on affected basis functions using the updated linear system $A(S)$.

The prolongated solution $\mathcal{P}p_c$ is usually a qualitatively correct approximation to p_f. To also control the residual of the approximation, we can cast the multiscale method into a two-level iterative solver,

$$\begin{aligned} p^{\nu+1/2} &= p^{\nu} + \mathcal{S}(q - Ap^{\nu}) \\ p^{\nu+1} &= p^{\nu+1/2} + A_c^{-1}(q - Ap^{\nu+1/2}), \end{aligned} \tag{11}$$

where ν is an iteration parameter and $\mathcal{S}$ is some inexpensive smoother like ILU.

3.2. Preserving Vorticity

Vorticity is a vector that describes the rate and direction of rotation of a fluid particle at any given point. Mathematically, it is defined as the curl of a velocity field

$$\vec{\omega} = \vec{\nabla} \times \vec{v}_t = (\frac{\partial v_3}{\partial x_2} - \frac{\partial v_2}{\partial x_3})\vec{i}_1 + (\frac{\partial v_1}{\partial x_3} - \frac{\partial v_3}{\partial x_1})\vec{i}_2 + (\frac{\partial v_2}{\partial x_1} - \frac{\partial v_1}{\partial x_2})\vec{i}_3, \tag{12}$$

and it is often used in fluid dynamics to show the structure of complex flows in an open medium filled by a single fluid. Using indexing from continuum mechanics, each component can be stated as

$$\omega = \frac{\partial v_i}{\partial x_j}\epsilon_{ijk}, \tag{13}$$

where ϵ_{ijk} is the *Levi–Civita* symbol, defined as a scalar triple product of unit vectors in a right-handed coordinate system, i.e., $\epsilon_{ijk} \equiv \vec{x}_i(\vec{x}_j \times \vec{x}_k)$. To display representative distributions of vorticity, it is sufficient to consider a single-phase velocity field

$$\vec{v}_t = -\mathbf{K}\nabla p, \tag{14}$$

where $\mathbf{K} = [K_{rs}]$ and $\nabla p = (\frac{\partial p}{\partial x_r}\vec{i}_r)$ are permeability tensor and pressure gradient, respectively. Inserting (14) into (13) and applying simple algebraic operations, we obtain

$$\omega_i = v_s\Big(\frac{\partial K_{kr}}{\partial x_j}\tilde{K}_{rs}\Big)\epsilon_{ijk} - K_{kr}\Big(\frac{\partial^2 p}{\partial x_j \partial x_r}\Big)\epsilon_{ijk}, \tag{15}$$

where $\mathbf{K}^{-1} = [\tilde{K}_{rs}]$ is the inverse permeability tensor. To keep mathematical operations as simple as possible, the permeability tensor is considered to be aligned with the coordinate axes so that off-diagonal elements of $\mathbf{K}$ are zero

($K_{ij} = 0$ for $i \neq j$), and diagonal elements of $\mathbf{K}^{-1}$ are given by $\tilde{K}_{ii} = 1/K_{ii}$. Hence, we can write (15) in a simplified format as

$$\omega_i = \sum_{\ell=1}^{3} \Big(v_\ell \frac{\partial \ln (K_{\ell\ell})}{\partial x_j} \epsilon_{ij\ell} - K_{\ell\ell} \frac{\partial^2 p}{\partial x_j \partial x_\ell} \epsilon_{ij\ell} \Big). \tag{16}$$

In this equation, ℓ is not a dummy index, and thus $K_{\ell\ell}$ is a nonzero diagonal element.

In a homogenized isotropic medium, we can assume $\frac{\partial^2 p}{\partial x_j \partial x_\ell} \epsilon_{ij\ell} = 0$ [45], so that (16) simplifies to,

$$\omega_i = v_\ell \frac{\partial \ln K}{\partial x_j} \epsilon_{ij\ell}. \tag{17}$$

By inserting $-\vec{i}_\ell \times \vec{i}_j = \epsilon_{ij} \vec{i}_i$ into (17), the vorticity vector can be correlated as $\omega_i = -(v_\ell \vec{i}_\ell) \times \frac{\partial \ln K}{\partial x} \vec{i}_j$, and stated as follows [34, 32]:

$$\vec{\omega}_i = -\vec{v}_t \times \vec{\nabla} \ln K. \tag{18}$$

Within petroleum engineering, vorticity was first used to model multiphase flow by [46]. Other researchers use a vorticity-stream function to simulate immiscible and miscible displacement [47]. White and Horne [48] were the first to publish the relation between permeability and vorticity, whereas Mahani and Muggeridge [32] were the first to use this concept for grid coarsening, which later proved to give effective and optimum coarse-scale grids [33].

It follows from (18) that single-phase vorticity captures variations in both permeability and velocity simultaneously. Indeed, vorticity would be high in the regions with a high velocity perpendicular to high permeability gradients. To accurately distinguish regions with significantly different flow behavior, it is crucial that the indicator is able to capture the connectivity and boundaries between regions with largely different permeabilities and flow rates. Systems with flow baffles is one such example. Figure 2 shows a low-permeability medium with a high-permeability channel (shown as a shaded region) inside which most of the flow will take place. Using permeability or velocity as indicator will cause agglomeration algorithms to coarsen cells *outside* the channel and retain the original resolution *inside*. A vorticity indicator, on the other hand, will only retain fine-scale cells along the channel borders.

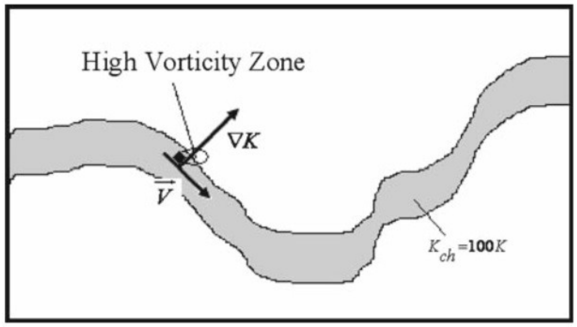

Figure 2: Embedded channel in a low-permeability porous media. The vorticity has maximum value on the channel boundaries, where most of ow takes place (permeability tensor is assumed diagonal and isotropic here).

4. Discussion and Numerical Results

The multiscale solver discussed above is implemented in the MATLAB Reservoir Simulation Toolbox (MRST, `http://www.mrst.no`) [49], which is an open-source framework that offers a comprehensive set of data structures, discretizations, workflow tools, as well as full simulators capable of running industry-grade simulations. Specifically, we use the MsRSB solver from MRST's `msrsb` module and a transport solver from the `incomp` module, whereas the routines for grid partitioning are the authors' own inhouse implementation.

This section presents numerical results for different test cases selected specifically to investigate potential benefits of adding a vorticity-based adaptive grid in the MsRSB method. To measure the discrepancy between multiscale pressure approximations and the corresponding fine-scale reference pressures, we use discrete L^2 and L^∞ norms:

$$\|p^{ms} - p^{fs}\|_2 = \sqrt{\frac{\sum_i |p_i^{ms} - p_i^{fs}|^2}{\sum_i |p_i^{fs}|^2}}, \tag{19}$$

$$\|p^{ms} - p^{fs}\|_\infty = \frac{\max_i |p_i^{ms} - p_i^{fs}|}{\max_i |p_i^{fs}|}. \tag{20}$$

Here, p^{ms} and p^{fs} are the multiscale and fine-scale pressure solutions, respec-

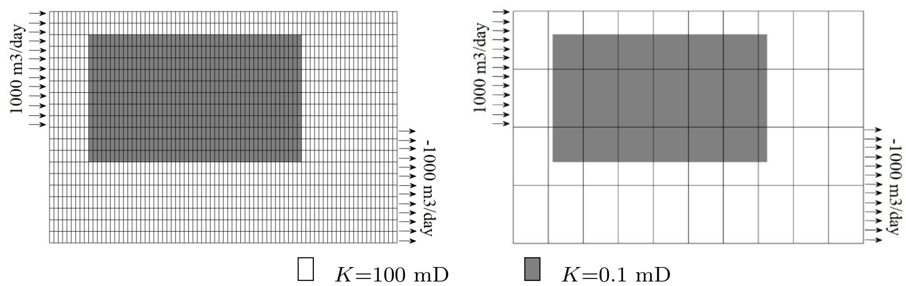

Figure 3: Lens model with fine-scale 80 × 20 grid (left) and coarse 10 × 4 partition (right). The uniform partition is generated so that the boundaries of the lens do not align with the coarse grid lines.

tively. Likewise, we introduce the saturation error:

$$\epsilon_{sat} = \frac{\sum_i \phi_i \, |S_i^{ms} - S_i^{fs}|}{\sum_i \phi_i S_i^{ms}}, \tag{21}$$

and define upscaling ratio (UR) as the ratio between the number of fine grid cells and the number coarse grid blocks.

4.1. Lens Model

The purpose of the first test case is to illustrate the difference in using permeability, velocity, and vorticity as indicator to generate adapted, nonuniform partitions. To this end, we consider a lens heterogeneity consisting of a rectangular, low-permeability region embedded in a high-permeability background; see Figure 3. The rock is initially fully saturated by a non-wetting fluid. We inject a wetting fluid at constant rate along the upper half of the west boundary and produce fluids at the same constant rate along the lower half of the east boundary. The way the injection is set up, the wetting phase will primarily move through the high-permeability zone and leave the non-wetting phase within the lens. The location and geometry of the lens has a significant impact on fluid flow, which our coarsening procedure should reflect.

Using logarithm of permeability as indicator generally identifies blocks having a large fraction of high-permeability cells as candidates for refinement. Here, the coarsening algorithm is set up so that only blocks that contain no lens cells

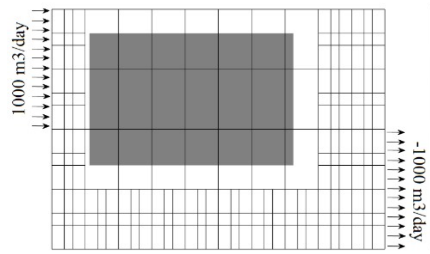

(a) Permeability indicator

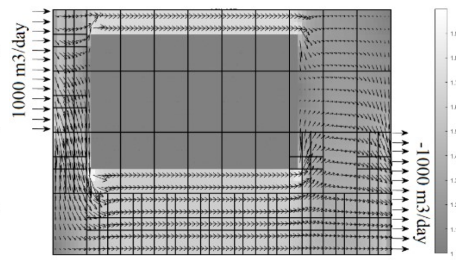

(b) Velocity indicator

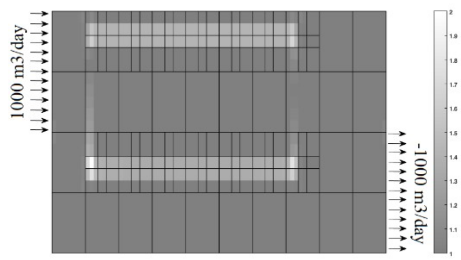

(c) Vorticity indicator

Figure 4: Comparison of coarse partitions adapting to three different indicators. (The white and black regions have the highest and the lowest values, respectively, and other regions are distributed regarding those values.)

are refined (Figure 4a). Almost one half of the initial coarse blocks are refined a factor 3×3, which means that the resulting number of coarse blocks is significantly higher than in the initial partition. This will increase the computational cost of each multiscale solve. It also worth to mention that this coarse grid does not change if we change the location of the inflow and outflow boundaries.

Using velocity as indicator also refines blocks in the high-permeability zone only, but gives significantly fewer coarse blocks as shown in Figure 4b. Unlike the permeability indicator, the velocity-based partition will change if we change the flow pattern. Since more flow information is used, we would expect to see an improvement in accuracy of the MsRSB simulation. However, as displayed in Figure 5, the saturation error is hardly reduced compared with the uniform case for coarse grids generated with permeability and single-phase velocity as indicators. On the other hand, using vorticity as indicator reduces the saturation

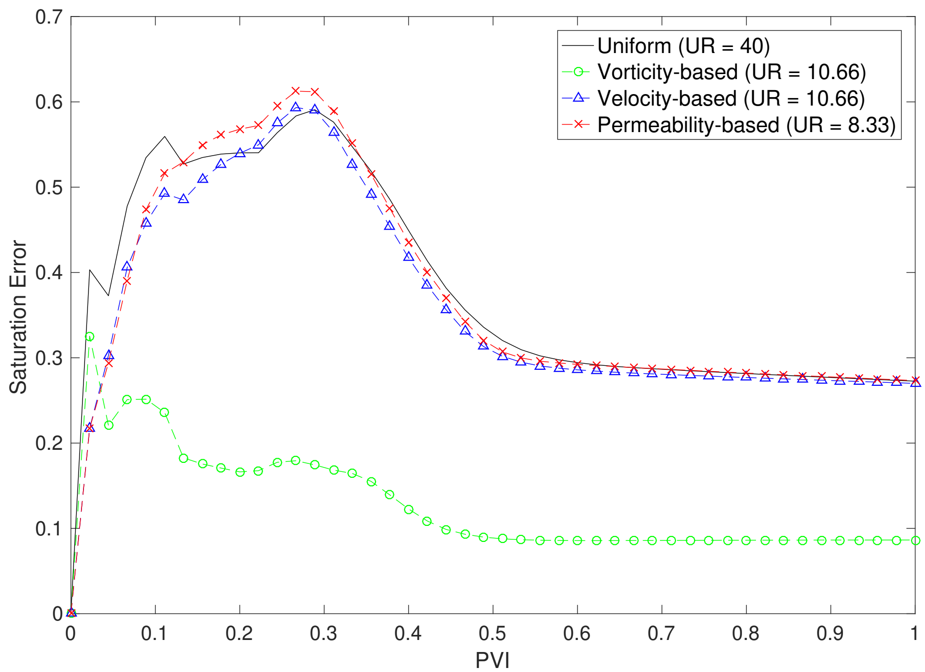

Figure 5: Comparison of saturation error for the lens model as function of dimensionless time (pore-volumes injected, PVI) for our different partitioning methods.

error significantly compared with the other three coarse grids. This supports our hypothesis that boundaries between regions with low permeability/flow and high permeability/flow are the most important to refine in the adaptive coarsening procedure. Capturing these zones is not possible unless we take both permeability and velocity effects into account, which (18) shows that vorticity really does. Therefore, vorticity-based coarsening results in refinement near the lens boundaries (Figure 4c) and gives a coarse grid with fewer blocks and higher accuracy than the other methods (see Figure 5).

4.2. SPE10 Model 2: Layer 43

Fluvial deposits typically give highly heterogeneous rocks with a wide range of heterogeneity scales. As an example of such heterogeneity, we pick Layer 43 from the Upper Ness section of Model 2 from the SPE10 benchmark [36]. This horizontal cross-section consists of a high-permeability channel connecting

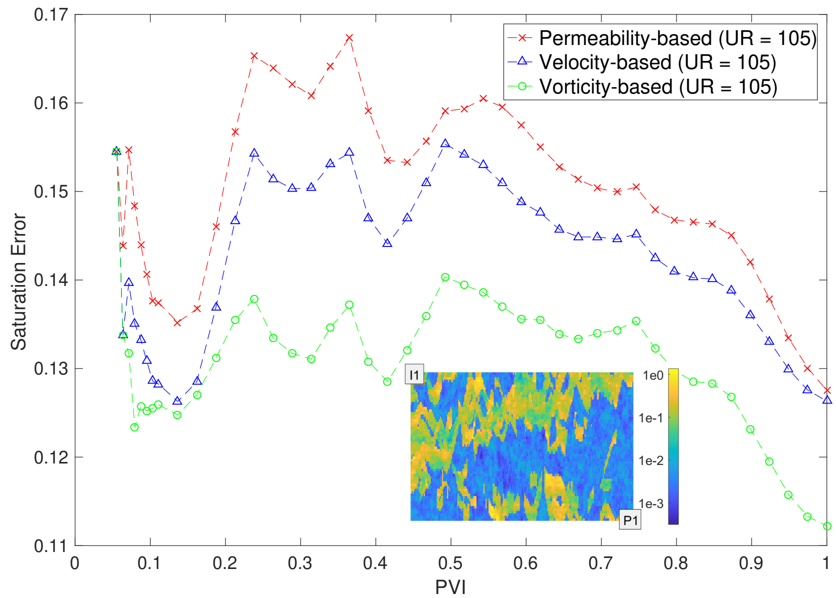

Figure 6: Saturation errors for a quarter-five spot setup on SPE10 Layer 43, simulated using MsRSB with three different coarse partitions.

from the left to the right. We place an injector (I1) in the northwest corner, operating at a constant injection rate of 4000 $\mathrm{m}^3/\mathrm{day}$, and a producer (P1) in the southeast corner, operating at a constant production rate of $-4000\ \mathrm{m}^3/\mathrm{day}$.

We use VMsRSB to run two-phase simulation on three coarse partitions generated in the same way as in the previous example. Figure 6 reports saturation errors relative to the fine-scale solution. Using vorticity as indicator clearly results in lower errors than using velocity, which in turn gives lower errors than using permeability. We also set up a five-spot well pattern on this layer with an injection well in the center and four producers in the corners. This arrangement is used for a two-phase simulation. Water cuts reported for the four producers in Figure 7 clearly show that MsRSB with vorticity as indicator is most successful in predicting water production rate at different wells. Overall, this confirms vorticity-based partitions improve the numerical accuracy of the multiscale solution.

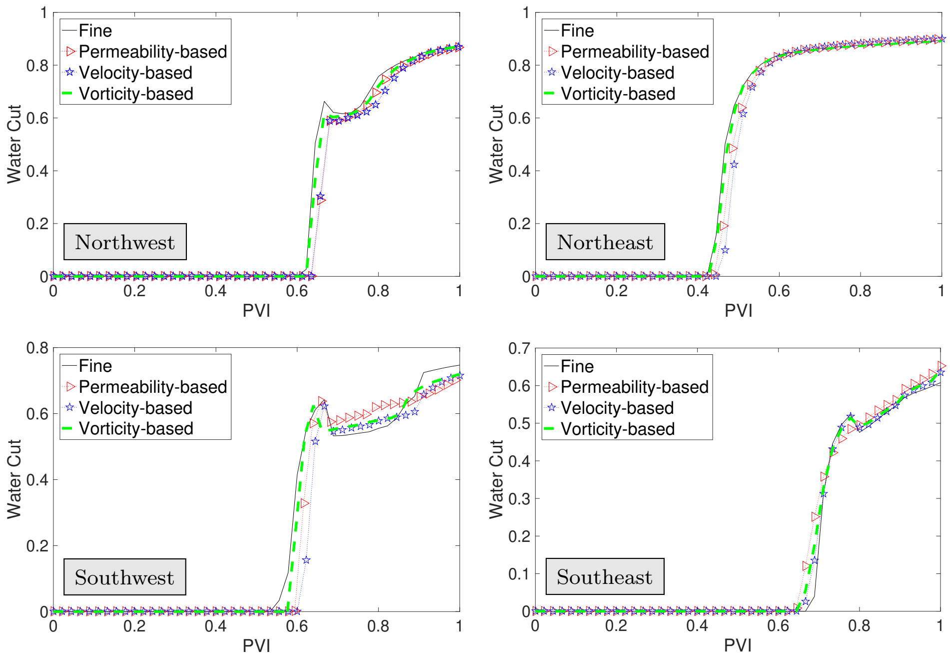

Figure 7: Water cuts for a five-spot setup on SPE10 Layer 43, simulated using MsRSB with three different coarse partitions.

4.3. SPE10 Model 2: All Layers

We now consider all layers of the SPE10 model, and generate three different partitions for each layer: a uniform 5×6 partition (UR=440), a vorticity-based refinement of the 5×6 partition (UR=110), and a 10×12 partition (UR=110). Figure 8 reports the pressure discrepancies measured in L^2 and L^∞ norm, as defined in Eqs. (19) and (20), for the three partitions. Points on the curves represent the mean value of the pressure discrepancy over all time-steps for each individual layer of SPE10. In addition, the straight solid lines give the mean pressure discrepancies over all layers. Although there are individual variations, the vorticity-adapted partitions improve the accuracy of MsRSB significantly compared with using a uniform partition. We interpret this to indicate that the coarse blocks selected for refinement contain influential details from fine cells that are not captured as well by the multiscale operators defined over a uniform partition.

We also observe that the vorticity-based partition generally gives better accuracy than the second structured partition, which has the same upscaling ratio (UR= 110). This supports our hypothesis that it generally is better to use an adapted partition that focuses the resolution of the coarse grids to transition zones between regions of high and low flow (and permeability). In other words, the accuracy of the multiscale method increases if its degrees-of-freedom are made denser in essential regions rather than spreading them uniformly out across the model. A fine-scale vorticity map can provide the information necessary to locate such regions.

On the coarse scale, the multiscale method effectively amounts to a multipoint discretization scheme because the support regions of two basis functions may overlap even if the corresponding coarse blocks do not share a common face. (Think of a 2D rectangular partition. The support of any basis function will overlap with the basis functions from the eight surrounding coarse blocks, and thus effectively give a 9-point scheme.) To further investigate the relative performance of the different partitions, we also compared the multiscale simulations to a fine-scale simulation with a multipoint scheme (from the `mimetic` module of MRST). The difference in performance is now smaller, but otherwise the trends are the same, and we therefore drop the plots for brevity.

4.4. 3D Models: The Norne and Johansen Formations

In the last example we apply the MsRSB and VMsRSB methods to two significantly more complex grid models: The first model uses the grid and petrophysical properties from a simulation model of the Norne oil field, whereas the second one uses the grid geometry from a sector model of the Johansen formation. Both models are given in the standard corner-point format, which in its basic form consists of hexahedral cells with a regular Cartesian topology. Our two models, however, contain faults, inactive cells, erosions, and so on, that induce complex unstructured connections and deformed and degenerate cell geometries. This means that cells have anything from 4 to 21 neighbors in the

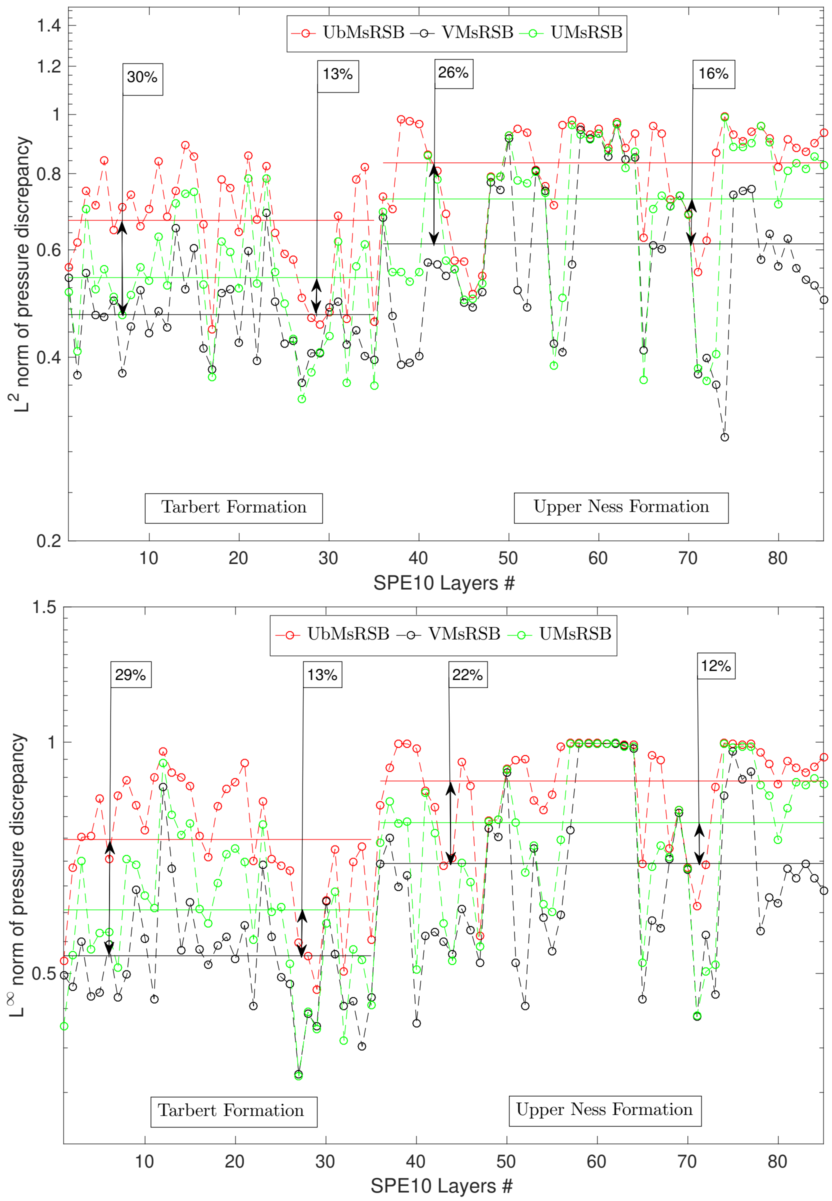

Figure 8: Mean pressure discrepancy over all time steps measured in L^2 (top) and L^∞ norm (bottom) for MsRSB simulations of all layers of SPE10 Model 2.

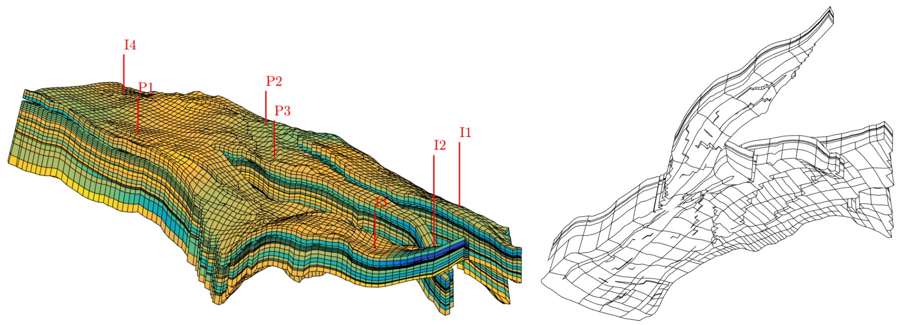

Figure 9: The Norne test case. The left plot shows the reservoir geometry and well positions, with cells colored by the lateral permeability using a logarithmic color scale. The right plot shows the refined coarse-scale grid generated using the vorticity indicator.

Norne model and between 4 and 14 neighbors in the Johansen model.

In 3D, the vorticity vector ($\vec{\omega}$) has three components, one in each axial direction, and we thus use the magnitude of this vector as our indicator. For each model, we perform one two-phase simulation with MsRSB with a load-balanced, rectangular partition (UR=91 for Norne, 33 for Johansen), and one simulation MsRSBE with a vorticity-based coarse-scale grid (UR=91 for Norne, 33 for Johansen). We also discuss how adding extra iterations in the pressure equation, see (11), can help the overall accuracy and computational efficiency.

Norne. The simulation model of the Norne oil/gas field, located in the Norwegian Sea, is one of the very few real simulation models that is freely available[1]. Herein, we only use the grid and petrophysical properties, and impose a relatively simple two-phase fluid and our own well arrangement consisting of four injection and three production wells, as depicted in Figure 9. The figure also shows the nonuniform partition generated by our vorticity-based method, which starts with a coarser partition than the load-balanced rectangular partition, but increases resolution locally to better resolve flow in regions of high vorticity. Figure 10 reports the discrepancies in saturation and pressure compared

[1]The Norne model is released as part of the Open Porous Media (OPM) initiative and can be downloaded from `github.com/OPM/opm-data`

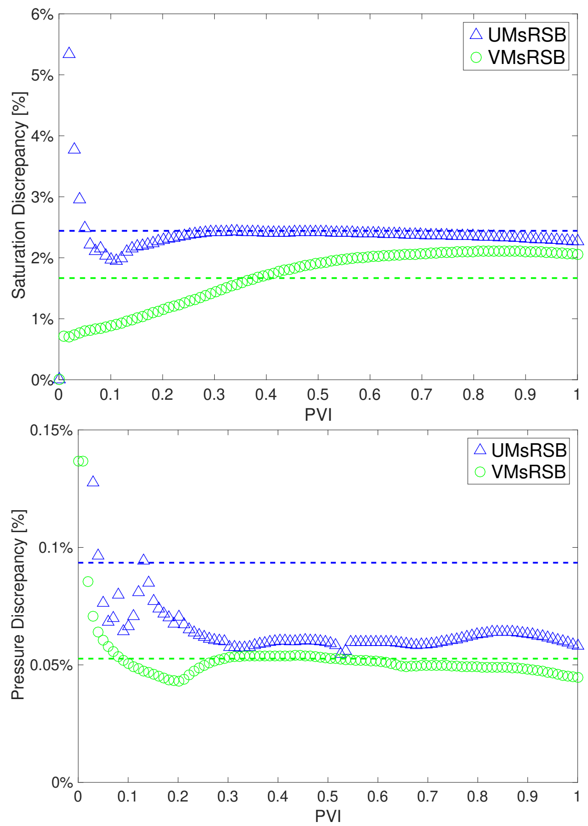

Figure 10: Discrepancy in saturation (top) and pressure (bottom) between a fine-scale simulation of the Norne test case and two MsRSB simulations with rectangular and vorticity-based partition, both with upscaling ratio UR=91. Dashed lines shows the average value for the corresponding data.

with a fine-scale simulation. We clearly observe that increasing grid resolution in regions of high vorticity and reducing grid resolutions elsewhere pays off in terms of increased accuracy for both pressure and saturation. Both multiscale simulations have the same number of degrees of freedom, but distribute them differently.

Figure 11 shows how using a few additional iterations in the multiscale solver drastically improves the accuracy of the pressure solution. The multiscale operator $\mathcal{RAP}$ is usually most effective during the first few iterations, before the smoother $\mathcal{S}$ takes over and ensures full convergence toward machine precision.

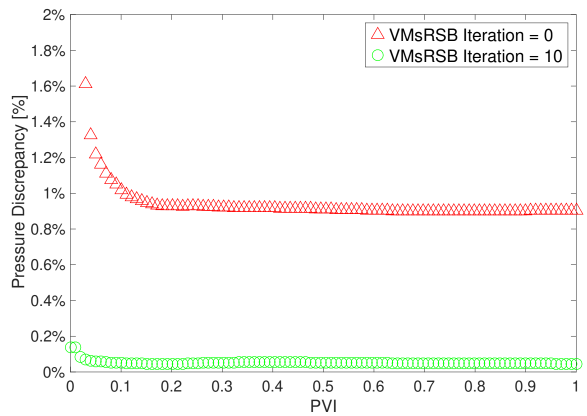

Figure 11: Reduction in pressure discrepancy achieved by iterating ten times on the MsRSB solver with vorticity-based partition for the Norne test case.

Using only a few iterations is therefore a good compromise between accuracy and computational cost for the pressure solves. Increased pressure accuracy is also beneficial for the transport equation (2) and tends to reduce the number of nonlinear iterations required during the transport steps, which in turns contributes to reduce the overall computational cost.

The Johansen Formation. The sector model of the Johansen formation shown in Figure 12 was originally created to study this formation as a candidate site for large-scale CO_2 storage offshore the south-west coast of Norway [50]. The petrophysical data follow a simple depth-correlated relationship and the formation has a rather narrow permeability range. To create a more challenging test case, we instead sample permeability randomly from the fluvial Upper Ness section of SPE10. The plot to the right in Figure 12 shows the coarse grid generated using vorticity-based partitioning. The regions around the injection and production wells have high vorticity and are therefore refined. Figure 13 reports discrepancies in saturation and pressure discrepancies compared with a fine-scale solution, and confirms the trend we observed for the Norne case.

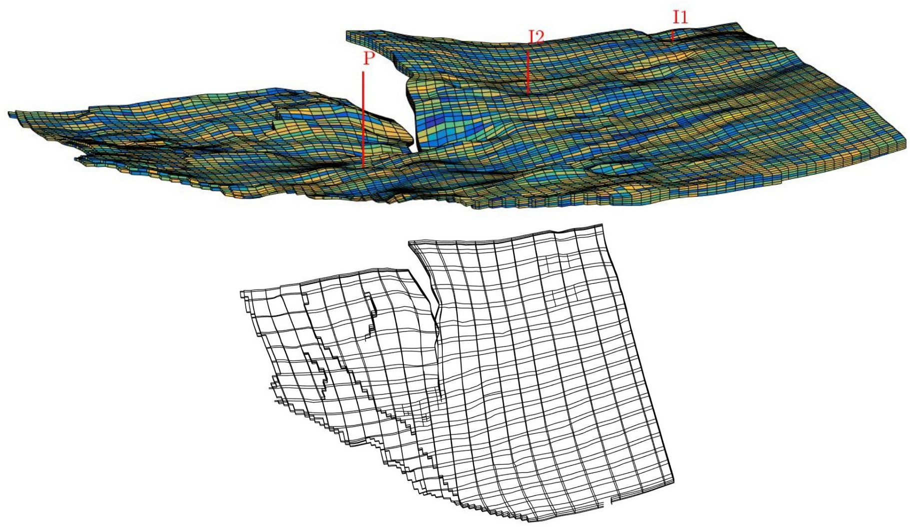

Figure 12: The Johansen formation with petrophysical properties sampled from the Upper Ness formation in the SPE10 Model 2 benchmark. The lower plot shows the corresponding vorticity-based partition.

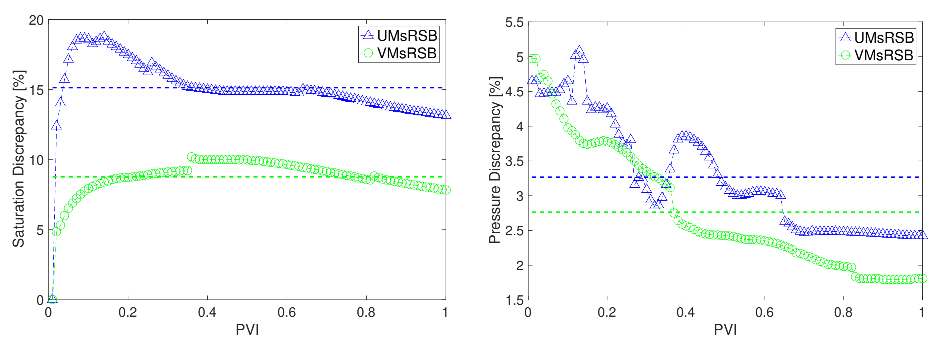

Figure 13: Discrepancy in saturation (left) and pressure (right) between a fine-scale simulation of the Johansen test case and two MsRSB simulations with rectangular and vorticity-based partition, both with upscaling ratio UR=33. Dashed lines shows the average value for the corresponding data.

5. Conclusion

We have proposed a combination of a state-of-the-art multiscale solver and a family of coarsening techniques that seek to adapt the resolution of the coarse partition to regions in the reservoir that have a strong impact on multiphase flow. Through a number of test cases, we have compared different indicators used to adapt the coarse partition. Our idealized 2D test cases consistently show that vorticity from a single-phase flow field is a better indicator than permeability and single-phase flow velocity. The advantage of this indicator is that it is able to locate transition zones having large gradients in both permeability and flow velocity. Our results indicate that it is more important to increase the resolution in these regions rather than only increasing the resolution in regions with high permeability or high velocity. Experiments with two 3D corner-point test cases indicate that the benefits of using vorticity-based partitions also carry over to more realistic scenarios. Vorticity-based partitions are relatively simple to generate for grids with structured connections and are prime candidate to be included as part of a multiscale–multibasis iterative solver framework [25, 51].

Appendix A. Numerical Procedure for Calculating Vorticity

We compute the single-phase vorticity indicator as the curl of a single-phase velocity. First, we reconstruct components of the velocity in direction of x_1 and x_2 from the inter-cell flux on the fine-scale grid cell computed by a standard two-point discretization in MRST [49]. Then, we use components of the velocity and cell center coordinates as inputs for MATLAB's curl function (as presented in (12)). This gives a single-phase vorticity map that may contain negative values due to direction changes in the velocity vector. Figure A.1 depicts the calculation. The final vorticity indicator is defined as the logarithm of the vorticity, shifted to positive values:

$$\mathrm{Vor}_{ind} = \log(|\omega|) - min(\log(|\omega|)) + 1. \tag{A.1}$$

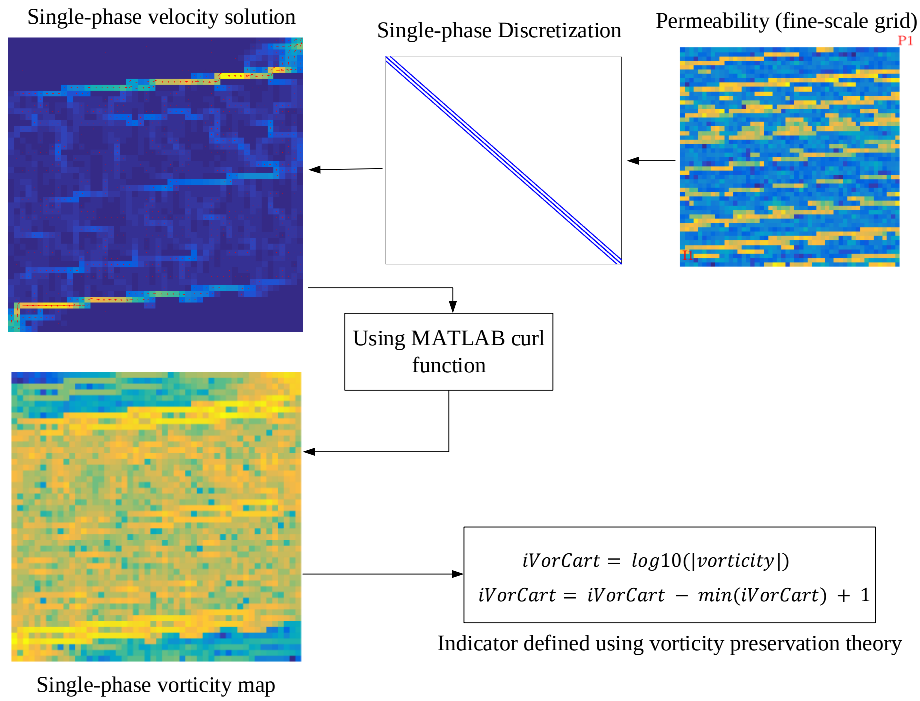

Figure A.1: Calculation of the single-phase vorticity indicator.

References

[1] T. Y. Hou, X.-H. Wu, A multiscale finite element method for elliptic problems in composite materials and porous media, Journal of Computational Physics 134 (1) (1997) 169–189 (jun 1997). doi:10.1006/JCPH.1997.5682.

[2] T. Arbogast, Implementation of a locally conservative numerical subgrid upscaling scheme for two-phase darcy flow, Computational Geosciences 6 (3) (2002) 453–481 (2002). doi:10.1023/A:1021295215383.

[3] T. Arbogast, K. Boyd, Subgrid upscaling and mixed multiscale finite elements, SIAM Journal on Numerical Analysis 44 (3) (2006) 1150–1171 (jan 2006). doi:10.1137/050631811.

[4] Z. Chen, T. Y. Hou, A mixed multiscale finite element method for elliptic

problems with oscillating coefficients, 541–576 72 (242) (2002). doi:10.1090/S0025-5718-02-01441-2.

[5] J. E. Aarnes, V. Kippe, K.-A. Lie, Mixed multiscale finite elements and streamline methods for reservoir simulation of large geomodels, Advances in Water Resources 28 (3) (2005) 257–271 (mar 2005). doi:10.1016/J.ADVWATRES.2004.10.007.

[6] P. Jenny, S. H. Lee, H. A. Tchelepi, Multi-scale finite-volume method for elliptic problems in subsurface flow simulation, Journal of Computational Physics 187 (1) (2003) 47–67 (may 2003). doi:10.1016/S0021-9991(03)00075-5.

[7] T. Arbogast, G. Pencheva, M. F. Wheeler, I. Yotov, A multiscale mortar mixed finite element method, Multiscale Modeling & Simulation 6 (1) (2007) 319–346 (jan 2007). doi:10.1137/060662587.

[8] K. Lipnikov, J. D. Moulton, D. Svyatskiy, A multilevel multiscale mimetic (m3) method for two-phase flows in porous media, Journal of Computational Physics 227 (14) (2008) 6727–6753 (jul 2008). doi:10.1016/j.jcp.2008.03.029.

[9] K. A. Lie, O. Møyner, J. R. Natvig, A. Kozlova, K. Bratvedt, S. Watanabe, Z. Li, Successful application of multiscale methods in a real reservoir simulator environment, Computational Geosciences 21 (5-6) (2017) 981–998 (2017). doi:10.1007/s10596-017-9627-2.

[10] X.-H. Wen, J. Gómez-Hernández, Upscaling hydraulic conductivities in heterogeneous media: An overview, Journal of Hydrology 183 (1-2) (1996) ix–xxxii (1996). doi:10.1016/S0022-1694(96)80030-8.

[11] P. Renard, G. de Marsily, Calculating equivalent permeability: a review, Advances in Water Resources 20 (5-6) (1997) 253–278 (oct 1997). doi:10.1016/S0309-1708(96)00050-4.

[12] C. L. Farmer, Upscaling: A review, International Journal for Numerical Methods in Fluids 40 (1-2) (2002) 63–78 (2002). doi:10.1002/fld.267.

[13] Y. Chen, L. J. Durlofsky, M. Gerritsen, X. H. Wen, A coupled local-global upscaling approach for simulating flow in highly heterogeneous formations, Advances in Water Resources 26 (2003) 1041–1060 (2003). doi:10.1016/S0309-1708(03)00101-5.

[14] Y. Chen, L. J. Durlofsky, Adaptive local-global upscaling for general flow scenarios in heterogeneous formations, Transp. Porous Media 62 (2006) 157–182 (2006). doi:10.1007/s11242-005-0619-7.

[15] V. Kippe, J. E. Aarnes, K.-A. Lie, A comparison of multiscale methods for elliptic problems in porous media flow, Computational Geosciences 12 (3) (2008) 377–398 (2008). doi:10.1007/s10596-007-9074-6.

[16] O. Møyner, K. A. Lie, A multiscale restriction-smoothed basis method for high contrast porous media represented on unstructured grids, Journal of Computational Physics 304 (2016) 46–71 (jan 2016). doi:10.1016/j.jcp.2015.10.010.

[17] O. Møyner, K.-A. Lie, A multiscale restriction-smoothed basis method for compressible black-oil models, SPE Journal 21 (06) (2016) 2079–2096 (2016). doi:10.2118/173265-PA.

[18] A. Kozlova, Z. Li, J. R. Natvig, S. Watanabe, Y. Zhou, K. Bratvedt, S. H. Lee, A real-field multiscale black-oil reservoir simulator, SPE Journal 21 (06) (2016) 2049–2061 (2016). doi:10.2118/173226-PA.

[19] Y. Wang, H. Hajibeygi, H. A. Tchelepi, Algebraic multiscale solver for flow in heterogeneous porous media, Journal of Computational Physics 259 (2014) 284–303 (feb 2014). doi:10.1016/J.JCP.2013.11.024.

[20] A. Kozlova, D. Walsh, S. Chittireddy, Z. Li, J. Natvig, S. Watanabe, K. Bratvedt, A hybrid approach to parallel multiscale reservoir simula-

tor, in: ECMOR XV–15th European Conference on the Mathematics of Oil Recovery, 2016 (aug 2016). doi:10.3997/2214-4609.201601889.

[21] A. M. Manea, J. Sewall, H. A. Tchelepi, Parallel multiscale linear solver for highly detailed reservoir models, SPE Journal 21 (06) (2016) 2062–2078 (2016). doi:10.2118/173259-PA.

[22] R. Sablok, K. Aziz, Upscaling and discretization errors in reservoir simulation, Petroleum Science and Technology 26 (10-11) (2008) 1161–1186 (jun 2008). doi:10.1080/10916460701833863.

[23] M. Garcia, A. G. Journel, K. Aziz, Automatic grid generation for modeling reservoir heterogeneities, SPE Reservoir Engineering 7 (02) (1992) 278–284 (1992). doi:10.2118/21471-PA.

[24] L. Durlofsky, R. Behrens, R. Jones, A. Bernath, Scale up of heterogeneous three dimensional reservoir descriptions, SPE Journal 1 (03) (1996) 313–326 (1996). doi:10.2118/30709-PA.

[25] K.-A. Lie, O. Møyner, J. Natvig, Use of multiple multiscale operators to accelerate simulation of complex geomodels, SPE Journal 22 (6) (2017) 1929–1945 (2017). doi:10.2118/182701-PA.

[26] A. N. Guion, B. Skaflestad, K.-A. Lie, X.-H. Wu, Validation of a non-uniform coarsening and upscaling framework, in: SPE Reservoir Simulation Conference, Society of Petroleum Engineers, 2019 (2019). doi:10.2118/193891-MS.

[27] L. J. Durlofsky, R. C. Jones, W. J. Milliken, A nonuniform coarsening approach for the scale-up of displacement processes in heterogeneous porous media, Advances in Water Resources 20 (5-6) (1997) 335–347 (oct 1997). doi:10.1016/S0309-1708(96)00053-X.

[28] A. Castellini, Flow based grids for reservoir simulation, Ph.D. thesis, Stanford University (2001).

[29] J. E. Aarnes, V. L. Hauge, Y. Efendiev, Coarsening of three-dimensional structured and unstructured grids for subsurface flow, Advances in Water Resources 30 (11) (2007) 2177–2193 (nov 2007). doi:10.1016/j.advwatres.2007.04.007.

[30] V. L. Hauge, K.-A. Lie, J. R. Natvig, Flow-based coarsening for multiscale simulation of transport in porous media, Computational Geosciences 16 (2) (2012) 391–408 (2012). doi:10.1007/s10596-011-9230-x.

[31] H. Mahani, Upscaling and optimal coarse grid generation for the numerical simulation of two-phase flow in porous media, Ph.D. thesis, Imperial College London (2005).

[32] H. Mahani, A. H. Muggeridge, Improved coarse grid generation using vorticity, in: SPE Europec/EAGE Annual Conference, SPE, Madrid, 2005 (2005).

[33] M. A. Ashjari, B. Firoozabadi, H. Mahani, Using vorticity as an indicator for the generation of optimal coarse grid distribution, Transport in Porous Media 75 (2) (2008) 167–201 (2008). doi:10.1007/s11242-008-9217-9.

[34] M. Ashjari, B. Firoozabadi, H. Mahani, D. Khoozan, Vorticity-based coarse grid generation for upscaling two-phase displacements in porous media, Journal of Petroleum Science and Engineering 59 (3-4) (2007) 271–288 (nov 2007). doi:10.1016/J.PETROL.2007.04.006.

[35] B. Firoozabadi, H. Mahani, M. A. Ashjari, P. Audigane, Improved upscaling of reservoir flow using combination of dual mesh method and vorticity-based gridding, Computational Geosciences 13 (1) (2009) 57–78 (2009). doi:10.1007/s10596-008-9105-y.

[36] M. Christie, M. Blunt, Tenth spe comparative solution project: A comparison of upscaling techniques, SPE Reservoir Evaluation & Engineering 4 (04) (2001) 308–317 (2001). doi:10.2118/72469-PA.

[37] S. T. Hilden, O. Møyner, K.-A. Lie, K. Bao, Multiscale simulation of polymer flooding with shear effects, Transp. Porous Media 113 (1) (2016) 111–135 (2016). doi:10.1007/s11242-016-0682-2.

[38] S. Shah, O. Møyner, M. Tene, K.-A. Lie, H. Hajibeygi, The multiscale restriction smoothed basis method for fractured porous media, J. Comput. Phys. 318 (2016) 36–57 (2016). doi:10.1016/j.jcp.2016.05.001.

[39] O. Møyner, H. A. Tchelepi, A mass-conservative sequential implicit multiscale method for isothermal equation of state compositional problems, SPE Journal 23 (6) (2018) 2376–2393 (2018). doi:10.2118/182679-PA.

[40] M. Tene, S. B. M. Bosma, M. S. A. Kobaisi, H. Hajibeygi, Projection-based embedded discrete fracture model (pEDFM), Advances in Water Resources 105 (2017) 205–216 (2017). doi:10.1016/j.advwatres.2017.05.009.

[41] S. Bosma, H. Hajibeygi, M. Tene, H. A. Tchelepi, Multiscale finite volume method for discrete fracture modeling on unstructured grids (ms-dfm), Journal of Computational Physics 351 (2017) 145 – 164 (2017). doi:10.1016/j.jcp.2017.09.032.

[42] T. Praditia, R. Helmig, H. Hajibeygi, Multiscale formulation for coupled flow-heat equations arising from single-phase flow in fractured geothermal reservoirs, Computational Geosciences 22 (5) (2018) 1305–1322 (Oct 2018). doi:10.1007/s10596-018-9754-4.

[43] N. Castelletto, H. Hajibeygi, H. A. Tchelepi, Multiscale finite-element method for linear elastic geomechanics, J. Comput. Phys. 331 (2017) 337–356 (2017). doi:10.1016/j.jcp.2016.11.044.

[44] N. Castelletto, S. Klevtsov, H. Hajibeygi, H. A. Tchelepi, Multiscale two-stage solver for Biot's poroelasticity equations in subsurface media, Computational Geosciences 23 (2) (2019) 207–224 (Apr 2019). doi:10.1007/s10596-018-9791-z.

[45] G. De Josselin De Jong, Singularity distributions for the analysis of multiplefluid flow through porous media, Journal of Geophysical Research 65 (11) (1960) 3739–3758 (jun 1960). doi:10.1029/JZ065i011p03739.

[46] E. Meiburg, G. M. Homsy, Vortex methods for porous media flows, in: Proceedings of the Symposium on Numerical Simulation in Oil Recovery on Numerical Simulation in Oil Recovery, Springer-Verlag New York, Inc., New York, NY, USA, 1988, pp. 199–225 (1988).

[47] A. Riaz, E. Meiburg , Three-dimensional vorticity dynamics of miscible porous media flows, Journal of Turbulence 3 (2002) N61 (jan 2002). doi:10.1088/1468-5248/3/1/061.

[48] C. D. White, R. N. Horne, Computing absolute transmissibility scale heterogeneity, Symposium on Reservoir Simulation (1987) 209–220 (1987). doi:10.2118/16011-MS.

[49] K.-A. Lie, An introduction to reservoir simulation using MATLAB/GNU Octave: User guide for the MATLAB Reservoir Simulation Toolbox (MRST), Cambridge University Press, 2019 (2019).

[50] G. Eigestad, H. Dahle, B. Hellevang, F. Riis, W. Johansen, E. Øian, Geological modeling and simulation of CO2 injection in the Johansen formation, Comput. Geosci. 13 (4) (2009) 435–450 (2009). doi:10.1007/s10596-009-9153-y.

[51] Ø. S. Klemetsdal, O. Møyner, K.-A. Lie, Accelerating multiscale simulation of complex geomodels by use of dynamically adapted basis functions, Computational GeosciencesAccepted (may 2019).